Available online at www.sciencedirect.com

SciVerse ScienceDirect

Ceramics International 39 (2013) 813–818

CERAMICS INTERNATIONAL

www.elsevier.com/locate/ceramint

Hydrothermal synthesis and optical property of scale- and spindle-like ZnO

Narges Kiomarsipour*, Reza Shoja Razavi

Department of Materials Engineering, Malek Ashtar University of Technology, P.O. Box 83145/115, Shahin Shahr, Isfahan, Iran

Received 1 July 2012; accepted 1 July 2012
Available online 8 July 2012

Abstract

In the present work, well-dispersed two new structures of scale- and spindle-like ZnO were successfully synthesized by using zinc nitrate hexahydrate as the starting material and also the low temperature hydrothermal process and any additional surfactant, organic solvents or catalytic agent. The ZnO structures were characterized by X-ray diffraction (XRD), field-emission scanning electron microscopy (FE-SEM) and transmission electron microscopy (TEM). Optical property of the ZnO structures was investigated by room-temperature photoluminescence (PL) spectroscopy. The results revealed that ZnO powders have hexagonal (wurtzite-type) crystal structure and a large amount of well-dispersed ZnO scale- and spindle-like structures was formed. The thickness of scales was in the range 40–60 nm and the diameter of spindles was in the range 50–70 nm. Room-temperature PL spectra from the ZnO structures showed a weak UV emission peak at ~382 nm and a very strong visible green emission at ~530 nm, that was ascribed to the transition between V_oZn_i and valence band.

Keywords: D. ZnO; Hydrothermal synthesis; Morphology; Photoluminescence

1. Introduction

ZnO is a direct wide band gap (3.37 eV) semiconductor with a large excitonic binding energy (60 meV) at room temperature. Direct fabrication of special structures with controlled crystalline morphology represents significant challenge in various fields, because it can provide a better model for investigating the dependence of electronic and optical properties on the size confinement and dimensionality [1–4]. Various ZnO structures including nanobrushes [5], nanowires [6], nanobowls [7] and nanoplates [8] have been produced. They are widely used in many important areas, such as solar cells [9], pigments [10], gas sensors [11], electronics [12] and photocatalysts [13]. Different methods have been used to prepare ZnO nanostructures, such as hydrothermal [14], sol–gel [15], mechanical milling [16] and chemical vapor deposition [17]. All wet-chemical methods for preparation of ZnO nanostructures need to use organic solvents, surfactants, high temperatures, very hard process control and templates [18–21], whereas the hydrothermal method is a promising one for fabricating ideal structures with special morphology because of the low cost, low temperature, high yield and scalable process. In the present work, a simple hydrothermal process was used to prepare two novel well-dispersed ZnO nanostructuers on a large-scale at low-temprature and without using any additives.

2. Experimental

2.1. Synthesis of scale-like ZnO

In a typical experiment of synthesizing scale-like ZnO, 1.5 M zinc nitrate aqueous solution was prepared by adding 31.22 g $Zn(NO_3)_2 \cdot 6H_2O$ (Reagent Grade, 98% Sigma-Aldrich) to 50 mL distilled water. The pH of the solution increased to 11 by adding dropwise 2 M solution of KOH (11.22 g KOH added in 50 mL distilled water) and stirring vigorously for 10 min at room temperature. Then the resulting slurry mixture was transferred into a 100 mL Teflon-lined stainless steel autoclave up to 80% of the total

*Corresponding author. Tel.: +98 312 5225041; fax: +98 312 5228530.
E-mail addresses: na.kiomarsipour@yahoo.com (N. Kiomarsipour), shoja_r@mut-es.ac.ir (R. Shoja Razavi).

0272-8842/$36.00
http://dx.doi.org/10.1016/j.ceramint.2012.07.002

volume. Hydrothermal reaction was conducted at 160 °C for 18 h in an oven. After the reaction was completed, the final product was collected by pressure filtration. Powdered sample was thoroughly washed with distilled water and then dried in air at 120 °C for 12 h. Finally, about 2.88 g of product was harvested.

2.2. Synthesis of spindle-like ZnO

0.5 M zinc nitrate aqueous solution was prepared by adding 7.34 g $Zn(NO_3)_2 \cdot 6H_2O$ to 70 mL distilled water. The pH of the solution increased to 11 by adding 2 M solution of KOH dropwise and stirring vigorously for 10 min at room temperature. Then the resulting slurry mixture was transferred into a 100 mL Teflon-lined stainless steel autoclave. Hydrothermal reaction was conducted at 160 °C for 18 h in an oven. After the reaction was completed, the final product was collected by pressure filteration. Finally, about 1.85 g of product was harvested.

2.3. Characterization

Crystal structure of as-prepared products was characterized by powder X-ray diffraction (XRD) on a Bruker D8 Advance X-ray diffractometer using Cu-Kα radiation (40 kV, 40 mA and $\lambda = 0.1541$ nm). XRD patterns were recorded from 0° to 90° with a scanning step of 0.02 °/s. Morphology and size of the samples were analyzed by Hitachi S-4160 Field Emission Scanning Electron Microscopy (FE-SEM) at an accelerating voltage of 15 kV and the Philips CM10 transmission electron microscope (TEM), using an accelerating voltage of 200 kV. Room-temperature photoluminescence spectra (PL) were achieved on an Edinbergh instrument FLS 920 spectroscope using a 250 nm excitation line.

3. Results and discussion

Typical XRD patterns of the products are shown in Fig. 1a and b. All diffraction peaks can be indexed as hexagonal wurtzite ZnO with cell constants $a = 3.2490$ A° and $c = 5.2050$ A° for products, which is in good agreement with the reported data for ZnO of JCPDS File no. 00-005-0664. Very sharp diffraction peaks indicated the good crystallinity of the prepared crystals and no characteristic peaks were detected for the other impurities such as $Zn(NO_3)_2 \cdot 6H_2O$ and $Zn(OH)_2$.

The morphology and structural characterizations of the scale- and spindle-like ZnO are shown in Figs. 2 and 3. As can be seen in Figs. 2a and 3a, the products are composed of well-dispersed crystals with scale- and spindle-like structures on a large scale, where all the scales have fairly uniform diameters of about 300 nm and thicknesses of 50 nm. The diameters and lengths of spindle-like ZnO are about 70 nm and 1–2 μm, respectively. The magnified SEM images, shown in Figs. 2b, c and 3b, c, indicate the detailed morphology of the ZnO structures. The products

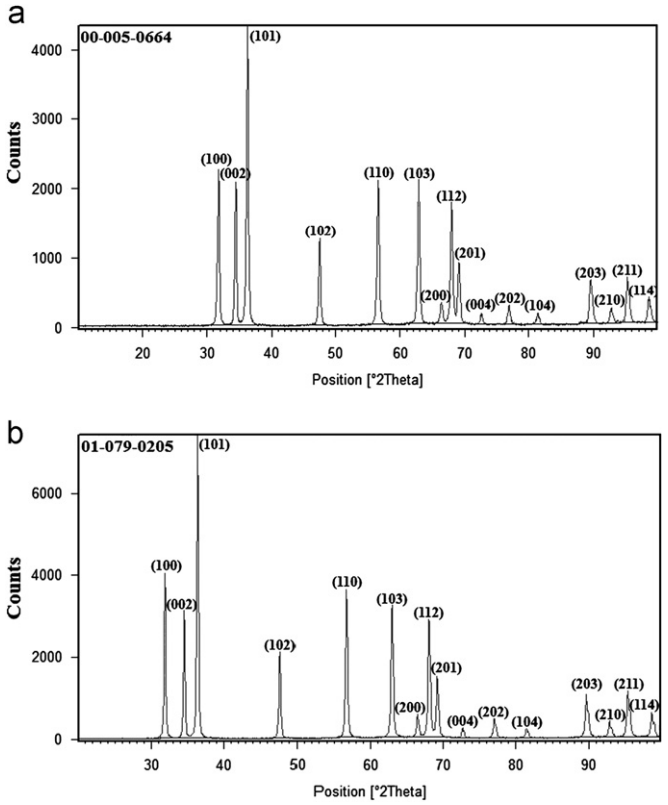

Fig. 1. XRD patterns of (a) ZnO scale-like and (b) ZnO spindle-like.

are further characterized by TEM. As shown in Figs. 2d, e and 3d, e, all of the dispersed samples on the TEM grids show scale- and spindle-like shapes, which confirm the SEM results.

The possible mechanism of the formation of scale-like ZnO can be discussed based on both its nucleation and growth stages. At the nucleation stage, the intrinsic crystal properties dominate the shape of the initial ZnO seeds, that is, platelet seeds. The formation process for ZnO nanopowders under hydrothermal condition can be represented as follows. Precursor of basic zinc nitrate hexahydrate $Zn(NO_3)_2 \cdot 6H_2O$ hydrolyzes, which induces the formation of zinc hydroxide ($Zn(OH)_2$) hydrosol (shown in reaction (1)). If the pH value in the aqueous solution is about 11, $Zn(OH)_2$ is the main composition. During the hydrothermal process, part of the $Zn(OH)_2$ colloids dissolves into Zn^{2+} and OH^- according to reaction (2). When the concentrations of Zn^{2+} and OH^- reach the supersaturation degree of ZnO, according to reaction (3), ZnO nuclei is formed. The growth units of $Zn(OH)_4^{2-}$ (according to reaction (4)) have a tetrahedron geometry. The reactions in the solution are shown below [22]:

$$Zn(NO_3)_2 \cdot 6H_2O + 2OH^- \rightarrow 4Zn(OH)_2 + NO_3^{2-} + H_2O \quad (1)$$

$$Zn(OH)_2 \rightarrow Zn^{2+} + 2OH^- \quad (2)$$

$$Zn^{2+} + 2OH^- \rightarrow ZnO + H_2O \quad (3)$$

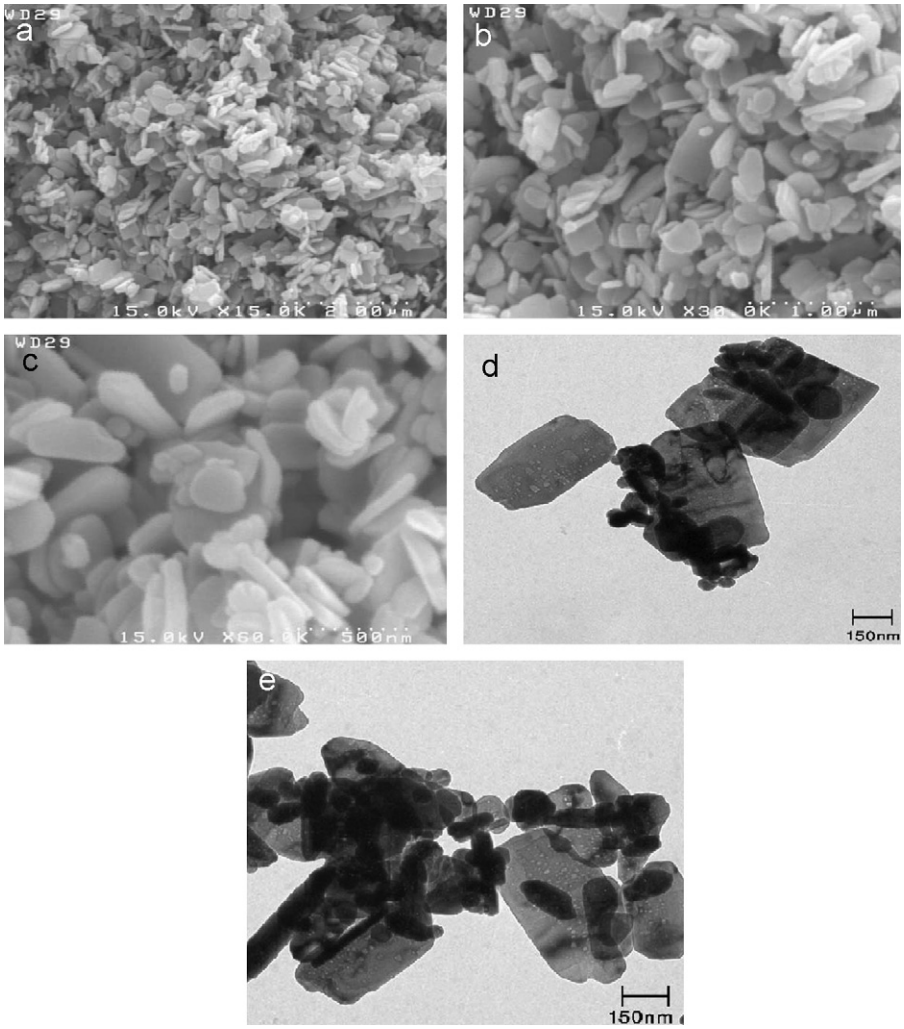

Fig. 2. (a) Low-magnification FE-SEM image, (b and c) high-magnification FE-SEM images and (d and e) TEM images of ZnO scale-like.

$$Zn(OH)_2 + 2OH^- \rightarrow Zn(OH)_4^{2-} \quad (4)$$

$$Zn(OH)_4^{2-} \rightarrow ZnO + H_2O + 2OH^- \quad (5)$$

The formation mechanism of crystals in solution mainly contains the formation of growth units and the incorporation of growth units into crystal lattice. The formation rate of ZnO nuclei is proportional to the concentration of the growth units $Zn(OH)_4^{2-}$ in solution. The formation rate of the growth unit is proportional to the concentration of Zn^{2+} and OH^- ions. So, the formation rate of ZnO nuclei is proportional to the concentration of Zn^{2+} and OH^- ions [23].

It can be seen from Figs. 2 and 3, that the morphology of the ZnO crystallite prepared by the hydrothermal method using different concentrations of $Zn(NO_3)_2 \cdot 6H_2O$ solution as precursors at 160 °C is greatly different. When the concentration of $Zn(NO_3)_2 \cdot 6H_2O$ solution is 1.5 M, the particle's morphology is scale-like and when the concentration of $Zn(NO_3)_2 \cdot 6H_2O$ solution is 0.5 M, the particle's morphology is spindle-like. In the scale-like morphology (Fig. 2), higher concentration led to high supersaturation and formation of many nuclei for the first time with small sizes. Formation of many nuclei caused reduction of supersaturation and inhibited grain growth. As the reaction was carrying out the concentration of precursor, the amount of growth units $Zn(OH)_4^{2-}$ in solution reduced, which could not provide sufficient raw materials for the growth of the nucleus. With higher concentration of Zn^{2+}, the nucleation rate would be higher. More nuclei formed in the initial stage would or may result in the formation of more ZnO scales, whereas in the spindle-like morphology (Fig. 3), lower concentration led to low supersaturation. Finally, after the nucleation stage, the growth units of $Zn(OH)_4^{2-}$ are subsequently incorporated into these seeds along the *c*-axis of ZnO crystal lattice and led to spindle-like morphology [24]. The schematic growth model of ZnO scale- and spindle-like structures is shown in Fig. 4.

The room-temperature PL spectra of as-prepared ZnO scale- and spindle-like, shown in Fig. 5a and b, were obtained with an excitation wavelenght of 250 nm. From Fig. 5, it can be seen that the as-produced samples exhibit a weak UV emission (380 nm) and a strong visible emission (530 nm).

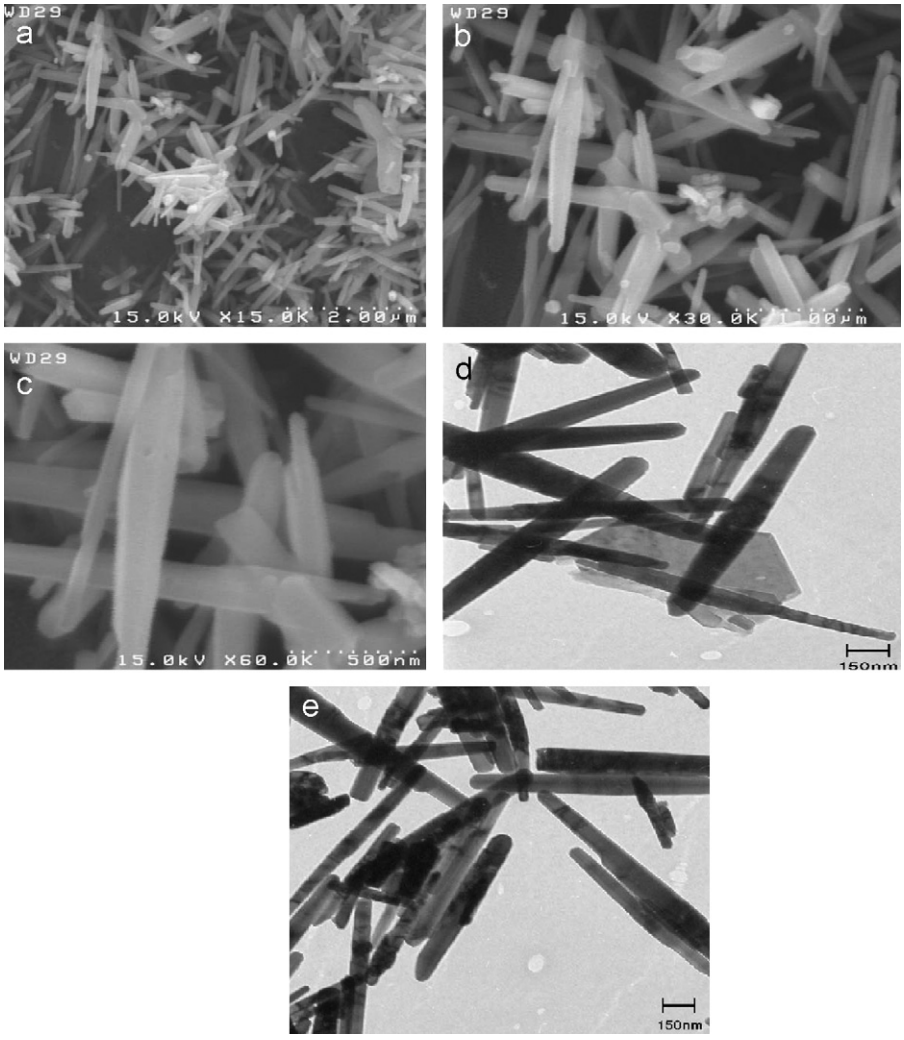

Fig. 3. (a) Low-magnification FE-SEM image, (b and c) high-magnification FE-SEM images and (d and e) TEM images of ZnO spindle-like.

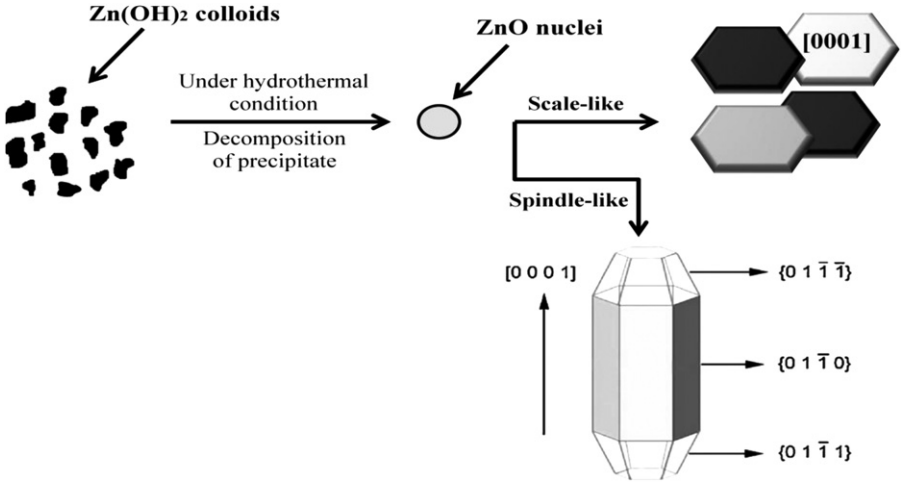

Fig. 4. The schematic illustration of the possible growth mechanism of ZnO scale- and spindle-like structures.

The weak UV peak at 3.26 eV corresponds to the near-band-edge (NBE) emissions originated from the recombination of the free excitons of ZnO. Furthermore, a strong visible emission, which is commonly due to different intrinsic or extrinsic defects, can also be found in the photoluminescence spectra of the as-produced samples [25].

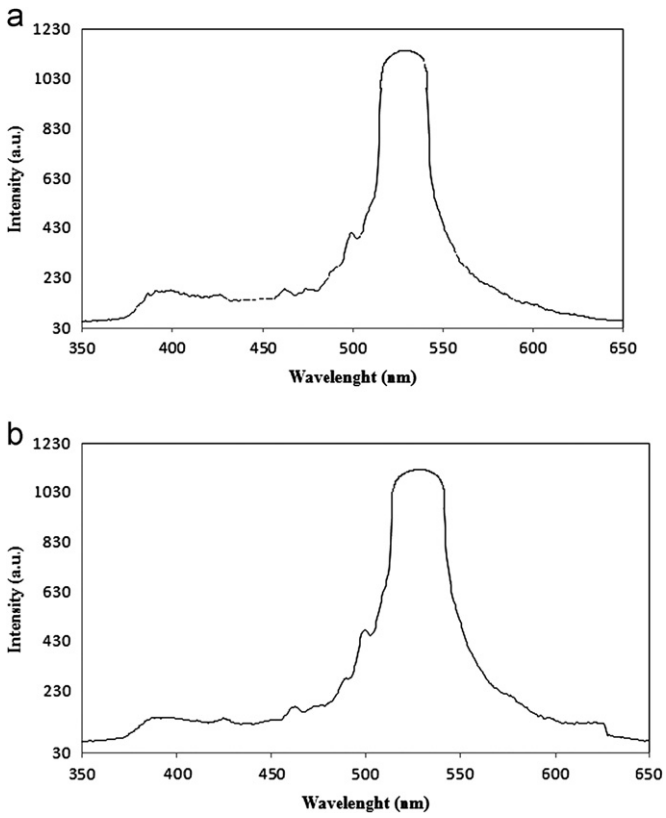

Fig. 5. Room-temprature photoluminescence spectra of (a) ZnO scale-like and (b) ZnO spindle-like.

The broad green emission band at about 530 nm is generally attributed to the radiative recombination of a photo-generated hole with an electron occupying the oxygen vacancy. However, surface states have also been identified as a possible cause of the visible emission in the ZnO nanomaterials. It is reasonable that there are some defects in the ZnO nanostructures at the surface and subsurface due to their fast reaction formation process and large surface-to-volume ratio [26]. Usually, the UV emission is attributed to the near band edge emission of the wide band gap of ZnO due to the annihilation of excitons. And the green luminescence is considered to be the result of radiative recombination of photo-generated holes with singularly ionized oxygen vacancies. In the present work, the stronger green emission should be attributed to much more defective of the microstructures prepared at lower temperature than those deposited at much higher temperatures, at which the UV emission is stronger [27,28]. Unlike those reported in many ZnO nanostructures synthesis, the green emission band (around 510–550 nm) due to the presence of the singly ionized oxygen vacancies (or other point defects) is clearly observable in our samples that was in accordance with the results of Wu et al. [29].

In the visible region, different peaks originate from different transitions. The peak on 525 nm relates to the transition between complex oxygen vacancy and interstitial zinc (V_oZn_i) and valence band, and the peak on 574 nm relates to the transition between complex oxygen vacancy and interstitial zinc (V_oZn_i) and valence band or between exciton level and antisite oxygen. It can be deduced that a very strong green emission band near 525 nm observed in the PL spectra of as-produced ZnO micro- and submicrorods should originate from the transition between V_oZn_i and valence band in ZnO structures [30].

4. Conclusions

Large-scale, well-dispersed scale- and spindle-like ZnO were successfully synthesized in a simple system at about 160 °C for 18 h by using the hydrothermal method. $Zn(NO_3)_2 \cdot 6H_2O$ and KOH were used as the reactants without using any additives. The structural analysis confirms that the as-syntesized ZnO structures are of hexagonal wurtzite phase. The results indicated that the concentration of starter solution has an important effect on the particles morphology and higher concentration of precursor led to smaller particles. The scale-like particles were obtained with 1.5 M zinc nitrate aqueous solution that are very uniform in size and morphology and suitable for pigmentation applications. The PL spectra of the products showed a very stong visible green emission at ~530 nm that is desirable in sensor industry.

References

[1] S.H. Ko, I. Park, H. Pan, N. Misra, M.S. Rogers, ZnO nanowire network transistor fabrication on a polymer substrate by low-temperature, all-inorganic nanoparticle solution process, Applied Physics Letters 92 (2008) 154102–154103.
[2] Y. Khan, S.K. Durrani, M. Mehmood, J. Ahmad, M.R. Khan, S. Firdous, Low temperature synthesis of fluorescent ZnO nanoparticles, Applied Surface Science 257 (2010) 1756–1761.
[3] Y.F. Zhu, W.Z. Shen, Synthesis of ZnO compound nanostructures via a chemical route for photovoltaic applications, Applied Surface Science 256 (2010) 7472–7477.
[4] L. Feng, A. Liu, J. Wei, M. Liu, Y. Ma, B. Man, Synthesis, characterization and optical properties of multipod ZnO whiskers, Applied Surface Science 255 (2009) 8667–8671.
[5] J. Wang, H. Zhuang, J. Li, P. Xu, Synthesis, morphology and growth mechanism of brush-like ZnO nanostructures, Applied Surface Science 257 (2011) 2097–2101.
[6] C.C. Lin, Y.Y. Li, Synthesis of ZnO nanowires by thermal decomposition of zinc acetate dihydrate, Materials Chemistry and Physics 113 (2009) 334–337.
[7] Y. Wang, X. Chen, J. Zhang, Z. Sun, Y. Li, K. Zhang, B. Yang, Fabrication of surface-patterned and free-standing ZnO nanobowls, Colloids and Surfaces A 329 (2008) 184–189.
[8] W.S. Chiu, P.S. Khiew, D. Isa, M. Cloke, S. Radiman, R.A. Shukor, M.H. Abdullah, N.M. Huang, Synthesis of two-dimensional ZnO nanopellets by pyrolysis of zinc oleate, Chemical Engineering Journal 142 (2008) 337–343.
[9] K. Keis, L. Vayssieres, S. Lindquist, A. Hagfeldt, Nanostructured Materials 12 (1999) 487.
[10] C. Li, Z. Liang, H. Xiao, Y. Wu, Y. Liu, Synthesis of $ZnO/Zn_2SiO_4/SiO_2$ composite pigments with enhanced reflectance and radiation-stability underlow-energy proton irradiation, Materials Letters 64 (2010) 1972–1974.

[11] J. Huang, Y. Wu, C. Gu, M. Zhai, Y. Sun, J. Liu, Fabrication and gas-sensing properties of hierarchically porous ZnO architectures, Sensors and Actuators B 155 (2011) 126–133.
[12] S.M. Peng, Y.K. Su, L.W. Ji, S.J. Young, C.N. Tsai, W.C. Chao, Z.S. Chen, C.Z. Wu, Semitransparent field-effect transistors based on ZnO nanowire networks, IEEE Electron Device Letters 32 (2011) 533–535.
[13] O. Akhavan, M.F Mehrabian, K. Mirabbaszadeh, R. Azimirad, Hydrothermal synthesis of ZnO nanorod arrays for photocatalytic inactivation of bacteria, Journal of Physics D: Applied Physics 42 (2009) 225305.
[14] Y. Wang, M. Li, Hydrothermal synthesis of single-crystalline hexagonal prism ZnO nanorods, Materials Letters 60 (2006) 266–269.
[15] R.S. Razavi, M.R. Loghman-Estarki, M.F. Khouzani, M. Barekat, Large scale synthesis of zinc oxide nano- and submicrorods by Pechini's Method: effect of ethylene glycol/citric acid mole ratio on structural and optical properties, Current Nanoscience 7 (2011) 807–812.
[16] S. Ozcan, M.M. Can, A. Ceylan, Single step synthesis of nanocrystalline ZnO via wet-milling, Materials Letters 64 (2010) 2447–2449.
[17] R. Bacsa, Y. Kihn, M. Verelst, J. Dexpert, W. Bacsa, P. Serp, Large scale synthesis of zinc oxide nanorods by homogeneous chemical vapour deposition and their characterization, Surface and Coatings Technology 201 (2007) 9200–9204.
[18] Y.H. Ni, X.W. Wei, J.M. Hong, Y. Ye, Hydrothermal preparation and optical properties of ZnO nanorods, Materials Science & Engineering B 121 (2005) 42–47.
[19] J. Wang, L. Gao, Hydrothermal synthesis and photoluminescence properties of ZnO nanowires, Solid State Communications 132 (2004) 269–271.
[20] Y. Wang, M. Li, Hydrothermal synthesis of single-crystalline hexagonal prism ZnO nanorods, Materials Letters 60 (2006) 266–269.
[21] J. Chen, H. Deng, M. Wei, Hydrothermal synthesis and optical properties of ZnO single-crystal hexagonal microtubes, Materials Science & Engineering B 163 (2009) 157–160.
[22] Y.X. Wang, J. Sun, X.Y. Fan, X. Yu, A. CTAB-assisted hydrothermal and solvothermal synthesis of ZnO nanopowders, Ceramics International 37 (2011) 3431–3436.
[23] W.J. Li, E.W. Shi, Y.Q. Zheng, Z.W. Yin, Hydrothermal preparation of nanometer ZnO powders, Journal of Materials and Science Letters 20 (2001) 1381–1383.
[24] B. Shouli, L. Xin, L. Dianqing, C. Song, L. Ruixian, C. Aifan, Synthesis of ZnO nanorods and its application in NO_2 sensors, Sensors and Actuators B 153 (2011) 110–116.
[25] C. Wu, H. Yu, Q. Huang, Y.C. Zhang, Synthesis of Sn-doped ZnO nanorods and their photocatalytic properties, Materials Research Bulletin 46 (2011) 1107–1112.
[26] Peng Zhiwei, Dai Guozhang, Chen Peng, Zhang Qinglin, Wan Qiang, Zou Bingsuo, Synthesis, characterization and optical properties of star-like ZnO nanostructures, Materials Letters 64 (2010) 90–898.
[27] Y.H. Ni, X.W. Wei, J.M. Hong, Y. Ye, Hydrothermal preparation and optical properties of ZnO nanorods, Materials Science & Engineering B 121 (2005) 42–47.
[28] Y. Sun, G.M. Fuge, M.N.R. Ashfold, Chemical Physics Letters 396 (2004) 21.
[29] C. Wu, X. Qiao, J. Chen, H. Wang, F. Tan, S. Li, A novel chemical route to prepare ZnO nanoparticles, Materials Letters 60 (2006) 1828–1832.
[30] S. He, M. Zheng, L. Yao, X. Yuan, M. Li, L. Ma, W. Shen, Preparation and properties of ZnO nanostructures by electrochemical anodization method, Applied Surface Science 256 (2010) 2557–2562.